



Failure behaviour of various pre-formed steel sheets with respect to the mechanical grain boundary properties

Roman Norz¹ · Simon Vitzthum¹ · Wolfram Volk¹

Received: 3 June 2021 / Accepted: 9 May 2022 / Published online: 15 June 2022
© The Author(s) 2022

Abstract

The forming history influences the mechanical properties and the formability of sheet metals. Numerous models and approaches have been published to implement this influence into FE-tools, based on isotropic damage or failure criterions. In this paper, the influence of a uniaxial pre-forming and a change in loading direction on the material parameters is investigated for two different steel grades in tensile tests. It was found, that a change in loading direction significantly affects the mechanical properties of the material. The force–displacement curves obtained from nanoindentation experiments were utilized to determine the flow curves for single grains as well as grain boundaries of the pre-formed materials. This was done by inverse parameter identification using finite element analysis.

Keywords Mechanical testing · Fracture · Microstructure · Grain boundaries · Anisotropic material

Introduction

Precise sheet metal forming simulations require a precise knowledge about the material behaviour. The material behaviour is often characterized by simple, monotonic experiments such as tensile, shear or biaxial tests. However, most sheet metal forming processes have a complex loading history which has to be taken into account. Various studies have been published in order to measure and model the material behaviour under complex loadings. Barlat et al. [1] investigated the influence of a uniaxial pre-forming on the mechanical parameters of a AA1050-O under various loading conditions. They found, that the height of the pre-forming influences the flow curve which is due to three effects. For low strains the Bauschinger effect plays an important role, followed by a reorganisation of dislocation structures and for larger strains texture evolution. It was shown, that the material parameters are strongly affected by a change in loading paths as well as the amount of pre-strain. Further investigations found, that a change in the loading direction with regard to the initial forming direction has a great influence on the material. Where Tarigopula et al. [25] found,

that the bigger the change in loading direction of a DP800 is, the bigger the difference in the transient behaviour is. Many approaches such as the Homogenous Anisotropic Hardening (HAH) model by Barlat et al. [2] or the crystal plastic models such as the Viscoplastic Self-Consistent Crystal Plasticity frame work (VPSC) by Lebensohn and Tomé [17] have been published to model the influence of pre-straining, change in load paths as well as the change in loading direction on the material behaviour, which was successfully used to simulate non-proportional loading of DP780 and CHSP45R by Kim et al. [14] and for a TRIP780 steel by Zaman et al. [33]. Next to these models also approaches using a mixed isotropic and kinematic hardening could be used to simulate non-proportional loading with a change in loading direction as done by Larsson et al. [16] for a DP600 and a DP1200. Most of these publications use interrupted experiments where the specimen is unloaded after a certain amount of pre-forming. Merklein et al. [19] were able to create strain paths with a continuous change in between different load cases. This was done by a biaxial test machine in combination with a cruciform specimen.

The influence of a change in loading direction for tensile tests of the mild steel DC05 and the aluminium alloy AA6016 was shown by Manopulo et al. [18]. It was found, that the DC05 steel is more sensitive to a change in loading direction compared to the AA6016. This effect is predicted well by a Modified Maximum Force Criterion (MMFC) in

✉ Roman Norz
roman.norz@utg.de

¹ Chair of Metal Forming and Casting, Technical University Munich (TUM), Munich, Germany

combination with a HAH model. A strong effect is also captured for the elastic–plastic transition of a DP800, where the strongest effect was captured for an orthogonal reloading of the material Tarigopula et al. [25].

The reason for this behaviour is found in the dislocations, the texture as well as the microstructure of the material (e.g. Barlat et al. [1]. By using TEM analysis Clausmeyer et al. [6] found, that for a DC06 steel cell walls begin to form at 5% deformation. When the material is further elongated until 12% deformation, almost all tangles are incorporated into cell walls or dense dislocation walls. An orthogonal loading of the pre-formed material leads to a change in the dislocation structure. Kim et al. [14] used a VPSC in combination with a dislocation-based hardening model (RGBV) to successfully predict the hardening behaviour as well as the anisotropy for a dual-phase steel DP780 and a single phase steel CHSP45R. The material parameters such as the recovery parameter, the back-stress parameter and others were found by a simplex optimization of a uniaxial tension–compression test data. For the dual-phase steel phase specific parameters are required for a sufficient accuracy. Vincze et al. [26] have investigated the mechanical behaviour in tensile tests after a uniaxial pre-forming for an AA1050-H24 aluminium alloy. For specimens with a change in loading over 45° an early softening of the material was found. Therefore, the texture is not the main source for the material response and further investigations on the microstructure have to be conducted. The VSPC models show, that a material model for different phases in a material are difficult to determine.

One way to obtain the parameters for material phases is nanoindentation. Choi et al. [5] used a spherical nanoindentation process to calculate the flow curve for both phases of a dual-phase steel. By indenting with two different indenter radii of 550 nm and 3.3 μm a sufficient accuracy of the flow curves was obtained. Seok et al. [22] used a similar procedure to determine the flow curves for pearlite and ferrite. Casals and Alcalá [4] deployed the force–displacement of a nanoindentation experiment with a Berkovich indenter by FE-simulation. They were able to determine the yield stress, Young's modulus and the strain hardening parameter by inverse parameter identification. For the FE-analysis the mesh size plays an important role, therefore, a sufficiently small size has to be chosen. Kim et al. [15] were able to define material parameters for different uniaxial pre-formed materials. An increase in hardness and decreasing strength coefficients and strain hardening exponents were observed for the investigated materials.

The forming history not only affects the mechanical parameters but also the formability of a material. Bergström and Ölund [3] investigated the influence on aluminium-killed steel (AK-steel) as well as one aluminium alloy. For both materials a significant influence

of pre-forming on the forming limit curve is found. The use of the Marciniak–Kuczynski model (M–K model) by Graf and Hosford [10] allowed the prediction of forming limits after pre-forming for an AA2008 T4 alloy which also showed a dependency on the pre-forming height and strain state (uniaxial, plane-strain and biaxial tension). To predict the forming limits of materials subject to non-proportional load paths Stoughton [23] has proposed a stress-based model which allows the path independent determination of forming limits which occurs for strain-based models. Nevertheless, a precise knowledge about the yield locus and the hardening behaviour is needed. This model was later extended to the Polar Effective Plastic Strain (PEPS) model, which does not show the strain-hardening limitations of the stress-based models, by Stoughton and Yoon [24]. Another stress-based approach is the Modified Maximum Force Criterion (MMFC) by Hora et al. [13] which has been extended multiple times Hora et al. [12], Hora and Tong [11]. The main idea is, that the strain state is shifted to a plain strain once the maximum force is reached. This model also requires profound knowledge about the stress–strain relationship of the material. To increase the robustness, a phenomenological approach, the so-called Generalized Forming Limit Concept (GFLC) was published by Volk et al. [28] and was further extended by Volk and Suh [31]. This approach uses a database consisting of bi-linear strain paths to determine the formability of an arbitrary non-proportional load path. For the database 72 experiments with different pre-strain heights and pre-strain states are needed. The GFLC is limited to strain paths with no change in loading direction. All the presented methods are based on isotropic damage behaviour. In recent findings it is found, that a change in loading direction significantly influences the formability and failure behaviour of a material in Nakajima experiments Volk et al. [30]. Therefore, the GFLC-model was extended to capture these effects as well by increasing the database which is needed. The proposed 3D-GFLC model by Volk et al. [27] was successfully verified by a novel tool and is able to predict the failure after non-proportional load paths with a change in loading direction.

In the present study, the reason for the anisotropic failure behaviour is further investigated. As the phenomenological 3D-GFLC model, based on macroscopic findings is able to predict this behaviour. The reasons for this behaviour are still not found yet. Therefore, a microscopic investigation of the microstructure is conducted for two steel grades, a micro-alloyed steel HC340LA and a mild steel DX56. To determine the influence of a change in loading directions the materials are uniaxial pre-formed. Followed by tensile tests without and with a change in loading direction. The influence on the mechanical parameters and the fracture strain are

determined. Using nanoindentation of the pre-formed materials and inverse parameter determination the flow curves of the grains and the grain boundaries were obtained.

Objective and solution strategy

In this paper, the results of Volk et al. [30] are further investigated. Nakajima experiments of pre-formed HC340LA steel under various loading directions showed a significant influence of the pre-forming and the change in loading direction on the necking strains. The failure could be separated in two types. Type I is the failure by localized necking, where Type II is a shear failure which corresponds with the early failure of the material, see Fig. 1. It was found, that an increase in void growth is responsible for the early failure of the material. By using a phenomenological model, this material behaviour was successfully predicted. The used 3D-GFLC model is an extension of the GFLC model by the parameter of loading direction and is also based on various experiments with different pre-forming heights, pre-forming states and changes in loading direction. Nevertheless, the reason for the increased void growth was not investigated. Vincze et al. [26] have found similar behaviour for AA1050

material in tensile tests which cannot be captured by the use of a VSPC model. They stated, that the texture is not the main source for the material behaviour and additional investigation on the microstructure has to be done.

Therefore, two steels with a very different microstructure, DX56 and HC340LA are uniaxial pre-formed and used in tensile tests under different loading angles.

Experimental setup

The investigated materials were a micro-alloyed steel HC340LA with an initial thickness of 1 mm and a mild steel DX56 with an initial thickness of 0.8 mm. Both materials are single phase steels, with only a ferrite phase present. Nevertheless, the two materials have a different microstructure regarding the grain size with the DX56 having a coarse microstructure and the HC340LA showing a fine microstructure, see Fig. 2.

To characterize the initial material, tensile tests were performed in 0°, 22.5°, 45°, 67.5° and 90° with respect to the rolling direction at a constant strain rate of 0.001 1/s. The forming limit curves were also determined for both materials to quantify the formability for different stress states using

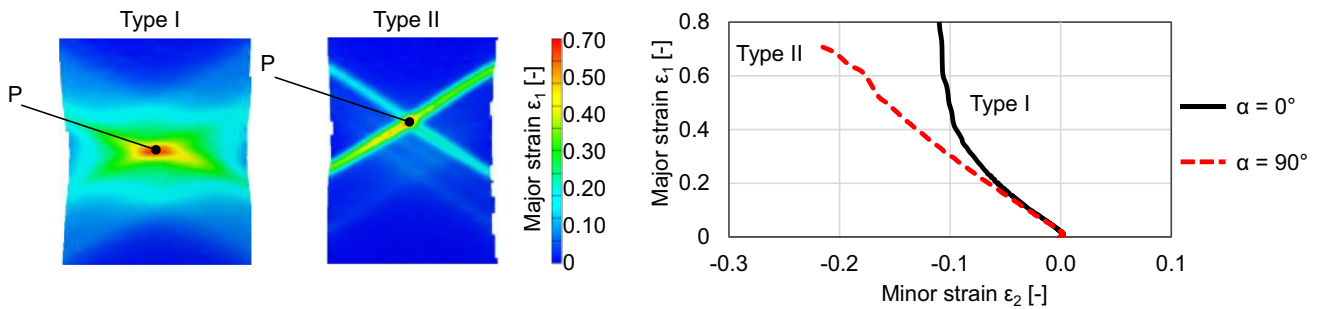
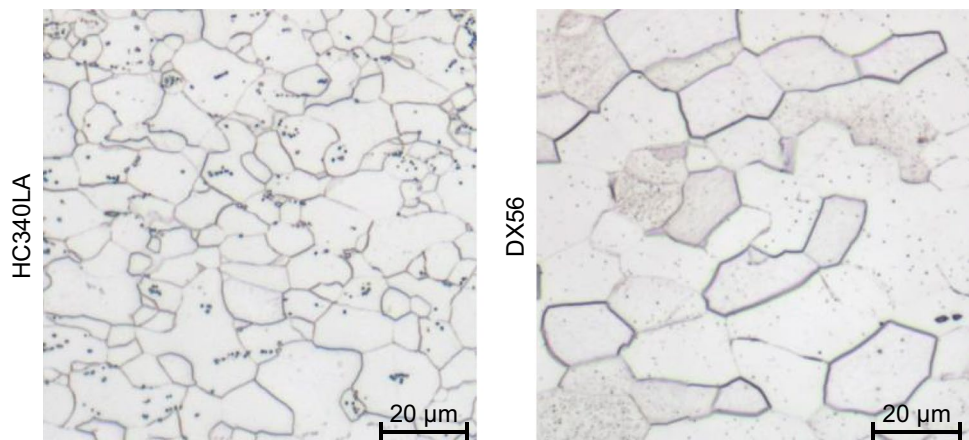


Fig. 1 Different failure types according to Volk et al. [30] for Nakajima specimens with no change in loading direction ($\alpha=0^\circ$) and a change in loading direction by 90° ($\alpha=90^\circ$)

Fig. 2 Microstructure of the HC340LA and the DX56 material



Nakajima tests with varying specimen widths at a constant punch speed of 1 mm/s. To reduce the friction, a PVC-pad in combination with a lubricant is used. For the tensile tests as well as the Nakajima experiments, at least three valid experiments were conducted.

Pre-straining of the materials

To create the non-proportional load paths, large stripes of the material were cut out and formed on a hydraulic press using an oversized Marciniak-tool developed by Weinschenk and Volk [32]. This tool was already successfully used to pre-form materials e.g. Volk et al. [27]. The punch speed was set to a constant value of 15 mm/s and deep drawing oil was applied on the specimens to reduce the friction between the punch and the specimens. By changing the drawing depth, the pre-forming height can be adjusted. All pre-forming specimens were cut out under 0° with regard to the initial rolling direction. For the pre-forming process in this investigation the use of a rectangular specimen geometry with a specimen width of 250 mm was sufficient as only uniaxial pre-forming states are investigated. If higher pre-forming heights or different pre-forming states, e.g. plane strain or biaxial, are needed, the specimen geometry has to be adapted. Due to the large, homogeneously pre-formed area with a diameter of 100 mm, see Fig. 3 (a), it is possible to extract five tensile test specimen out of one pre-formed rectangle. Prior to the forming process a grid was etched onto the material surface. After the first forming step, the deformed grid was measured to determine the pre-forming height. To measure the strains obtained by pre-forming, the optical measurement system ARGUS, which also allows the

determination of the strain distribution over a larger area, was used. The materials were pre-strained to six different pre-strain heights. For the specimen with a pre-forming of more than $\epsilon = 0.1$, the sheets were pre-formed in two consecutive steps with oil application in between the steps. This enables a more homogenous strain distribution even for high strains. The tensile tests were cut from the centre of the pre-formed specimen where the most homogenous strain distribution is found. The change in loading direction was done by rotating the tensile test geometry relatively to the initial forming direction where α denotes the angle between the initial forming direction and the subsequent loading direction, as shown in Fig. 3 (b). The final manufacturing process was done by milling.

Tensile tests

To ensure, that more tensile test specimens can be cut from a single pre-formed rectangle, the geometry H with a width of 12.5 mm as proposed in [8] was used. The measurement of the strain was done by a laser extensometer. The gauge length for the strain in longitudinal direction was set to 50 mm and a constant strain rate of 0.001 1/s was applied.

Nanoindentation

To identify the strength of the pre-strained microstructure, the flow curve of the ferrite grains as well as the grain boundaries are needed. Therefore, nanoindentation was done on the pre-formed materials to obtain the force–displacement curves. The indenter tip was a spherical punch with a radius of $5.8 \mu\text{m}$ and all experiments were conducted with a loading rate of 0.5 mN/s until a maximum force of 25 mN was reached. To minimize

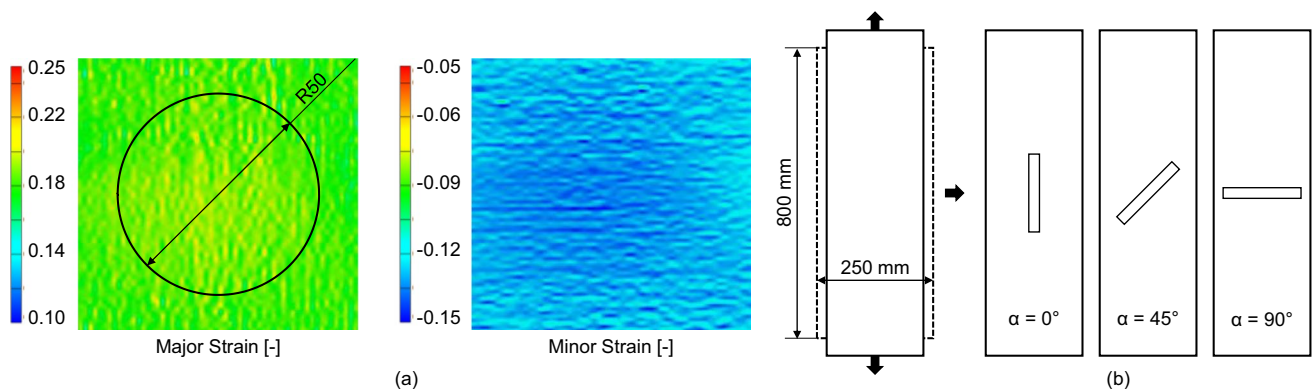


Fig. 3 **a** Homogeneity of the Major and Minor strain distribution of a DX56 specimen after pre-forming. **b** Specimen extraction from the pre-formed specimen and nomenclature of the tensile test specimens

the influence of the surface roughness, the material was polished and etched to make the grain boundaries visible. As the punch is smaller than the grain size for both materials, single ferrite grains could be tested. For testing the grain boundaries, indents were made at triple junctions of grain boundaries. This was done to ensure a sufficient grain boundary area to be tested.

Experimental results

Initial tensile tests and forming limit curves

Even though the two steel grades are both single phase ferrite steels, the stress–strain curves are very different. While the DX56 shows low strength and high ductility, the HC340LA has an increased strength and a lower ductility which is due to the smaller grain size of the material. The micro alloyed steel also shows a pronounced yield strength for all investigated angles with regard to the rolling direction. The onset of yielding is determined by the equivalent yield strength at 0.2% method (Rp0.2%). The mechanical parameters as well as the Forming Limit Curve are shown in Fig. 4. In between the different angles with regard to the rolling direction only small differences in the fracture strain (A50) and the uniform elongation (Ag) are visible. The forming limit curves of the material, obtained by using the time dependent evaluation method proposed by Volk and Hora [29], depict a good formability for both materials, where the DX56 shows a higher formability as expected for this very ductile steel grade.

Pre-straining and pre-formed tensile tests

Six different uniaxial pre-strain heights were investigated in this paper. The height of the pre-forming was chosen so that a large area between the onset of yielding and the uniform elongation is covered, see Table 1. It is noted, that even the highest pre-forming states are still below the uniform elongation for both materials, ensuring a sufficient remaining formability of the material before the onset of necking.

After a change in loading direction a loss of formability and an early onset of necking can be detected for both materials, while the onset of yielding remains unaffected. When the specimens are pre-formed higher than $\epsilon_{pre} = 0.05$, already a slight change in loading direction leads to an early necking indicated by uniform elongation and a decreased fracture elongation (Figs. 5, 6 and 7). Such a behaviour was also captured by Vincze et al. [26] for an AA1050 aluminium alloy which was uniaxial pre-formed up to 13.3%. A VSPC model was used to simulate this behaviour. When only the texture evolution due to the pre-forming is taken into account, these effects could not be captured. Therefore, additional investigations on the microstructure evolution are required.

Volk et al. [27] and Volk et al. [30], who investigated the same HC340LA in Nakajima experiments with two different pre-forming heights and three post-loading angles with respect to the initial forming direction, also found a significant loss of formability when the loading direction is changed, but this effect occurred only for pre-strains higher than those investigated in this paper. A separation in two different types of failure was done

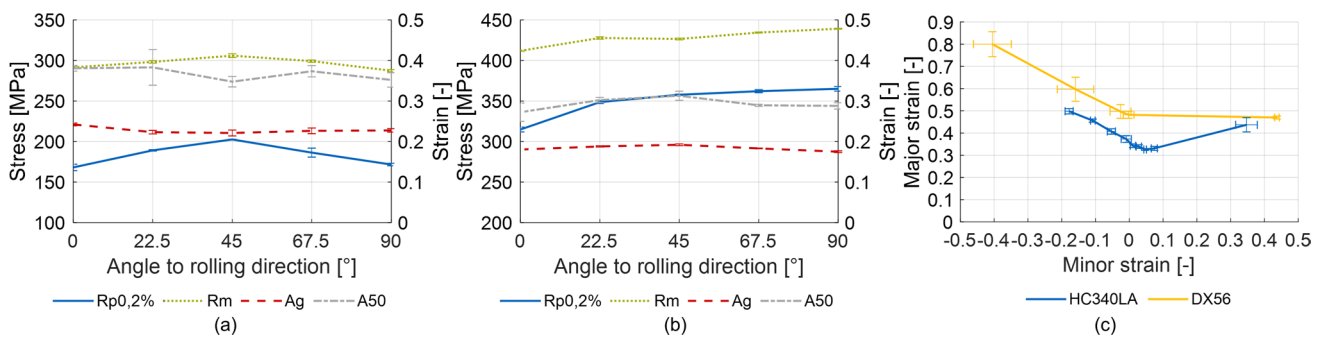


Fig. 4 Results of the initial tensile test with the (a) DX56 steel and (b) HC340LA steel and the forming limit curves for both materials

Table 1 Uniaxial pre-strain heights in logarithmic strain for the two materials

DX56	0.022 ±0.001	0.046 ±0.001	0.065 ±0.002	0.099 ±0.003	0.15 ±0.002	0.18 ±0.002
HC340LA	0.011 ±0.001	0.046 ±0.001	0.078 ±0.001	0.097 ±0.016	0.12 ±0.003	0.15 ±0.001

Fig. 5 Selected Stress–Strain curves for the two investigated materials HC340LA and DX56

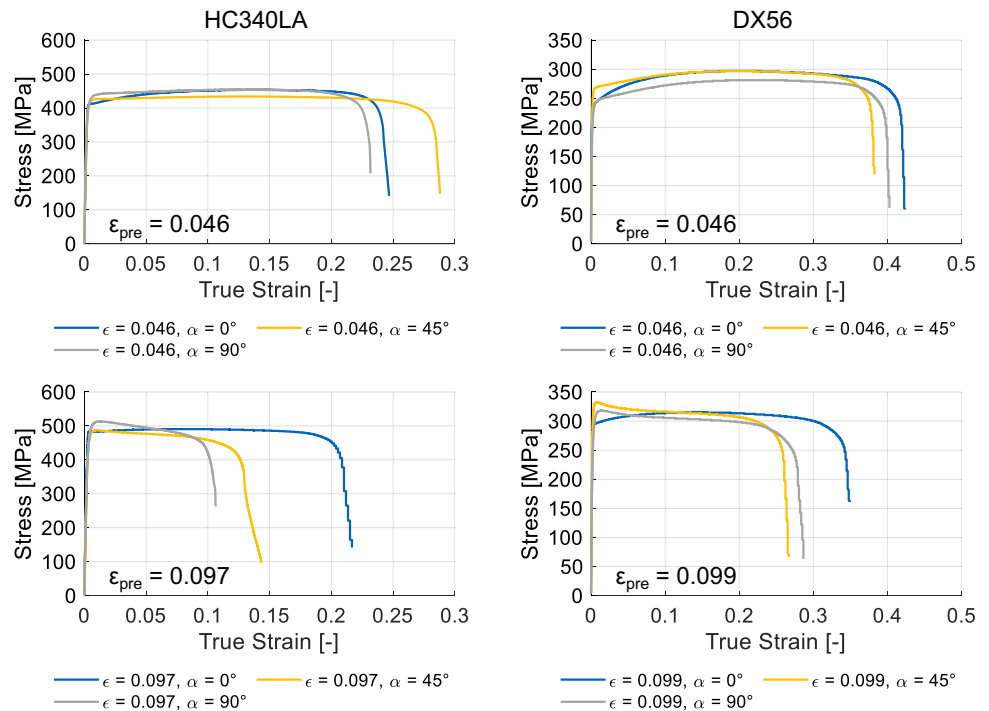
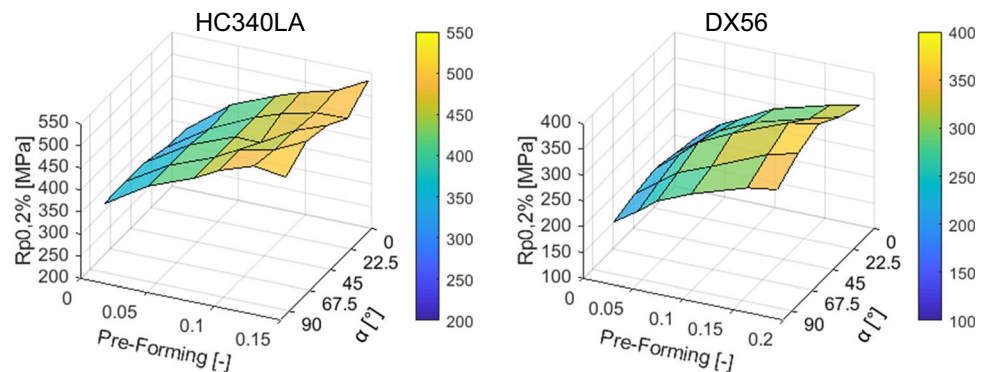


Fig. 6 Influence of pre-forming and a change in loading direction on the yield strength of HC340LA and DX56 determined by the Rp0.2%—method



where Type I indicates a failure by necking, while Type II indicates a shear failure.

At certain combinations of pre-forming height and change in loading direction, a mixed type can occur. The reason for this behaviour was found in an increased void growth for pre-formed materials with a change in loading direction. The different failure types are visible in Fig. 7.

By optical measurement of the occurring strains in tensile tests, the early localization of strain can be observed, shown in Fig. 8 and Fig. 9. The loss of global fracture elongation is therefore due this early localization, leaving the rest of the tensile test specimen almost undeformed. This localization area occurs randomly on the parallel length of the specimen, making it necessary to conduct more experiments to receive valid results. A closer look at the necking zone shows, that

the maximum strain close before fracture inside the necking zone is almost the same for the different pre-forming and angles α . The data from Fig. 6 and Fig. 7 can also be found in the appendix.

The strain path of the point P of each specimen is presented in Fig. 10. The strain path shows, that for the specimen with no change in loading direction ($\alpha = 0^\circ$) a shift from uniaxial tensile state to the plane-strain occurs, indicating a necking of the specimen. For the specimen with a change in loading direction ($\alpha = 90^\circ$), this change cannot be observed.

A closer look at the fracture surfaces reveals different fracture modes. For low pre-forming heights, the fracture surface shows a ductile fracture behaviour with void coalescence, regardless of the angle α for the

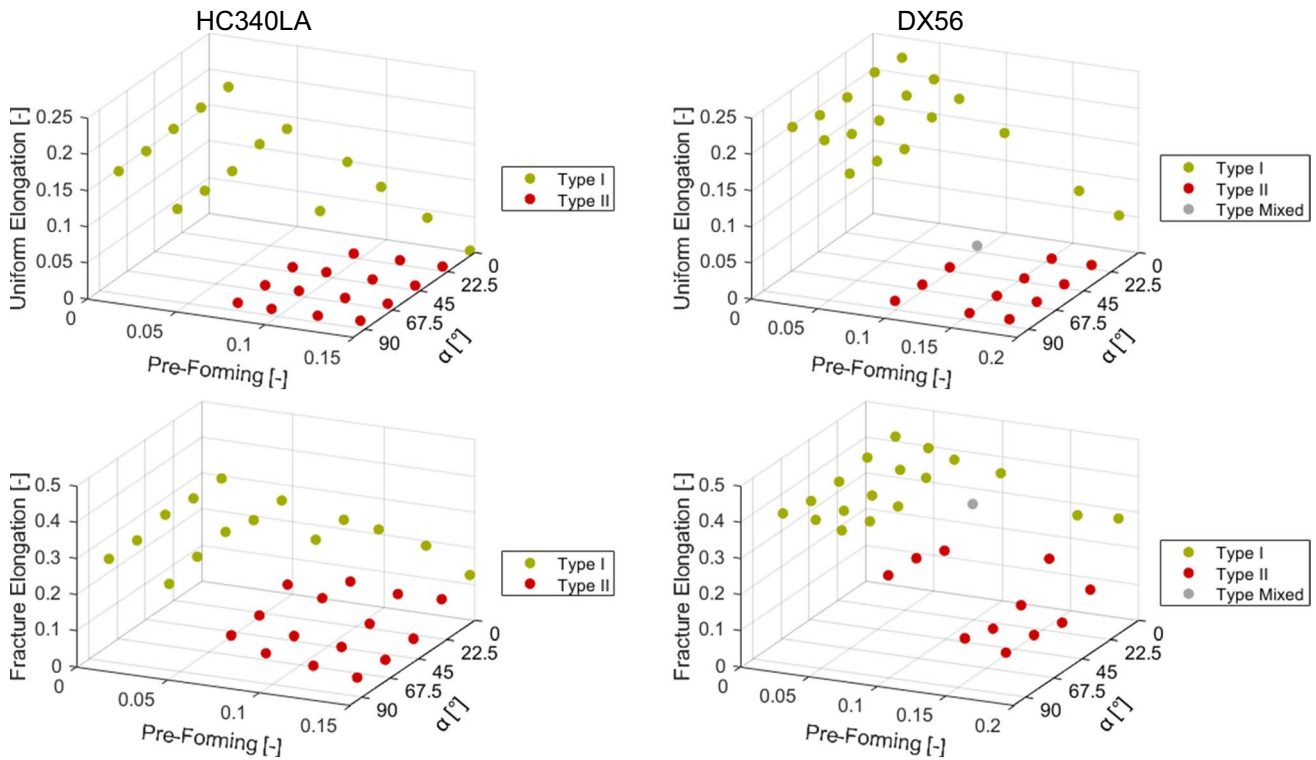


Fig. 7 Influence of pre-forming and the change in loading direction on the uniform and fracture elongation for the HC340LA and the DX56 steel, separated by the two failure types

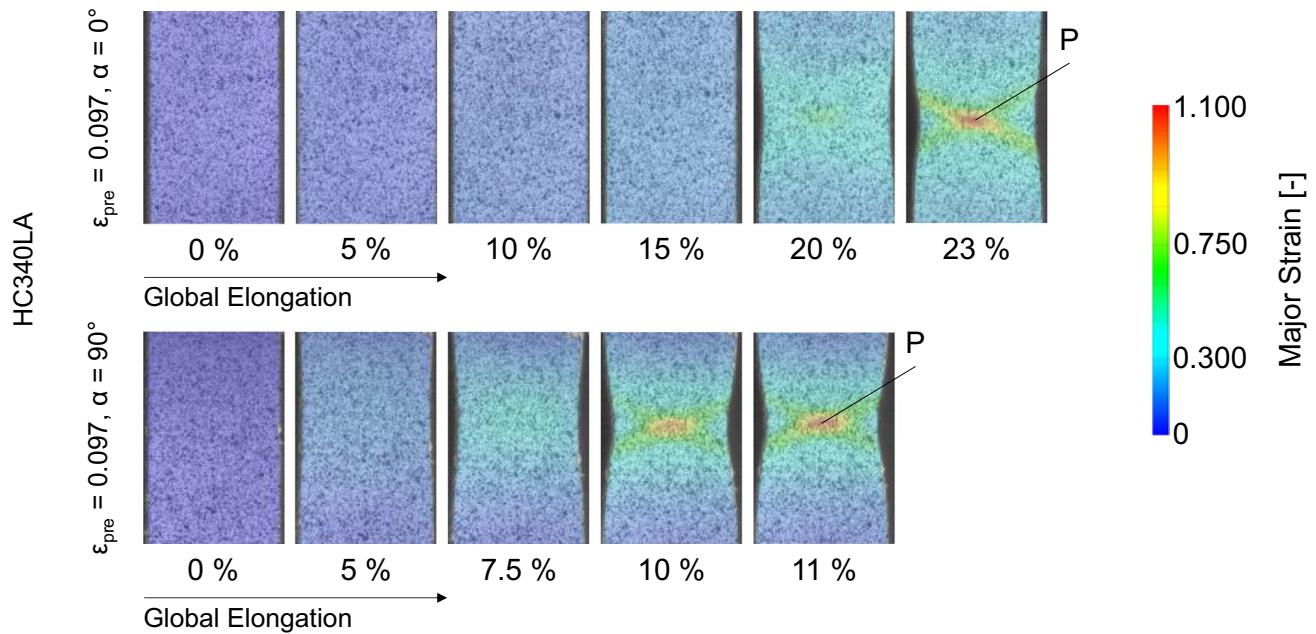


Fig. 8 Major Strain distribution for the HC340LA tensile test with a pre-forming of $\epsilon = 0.097$ and an angle of $\alpha = 0^\circ$ and $\alpha = 90^\circ$, respectively

HC340LA. When the pre-forming height is increased, the fracture mode changes when a change in loading direction occurs. An increase in void size is visible in Fig. 11.

After a pre-forming of $\epsilon = 0.097$, and a change in loading direction by $\alpha = 90^\circ$, the HC340LA materials show big voids. Between the voids a mixed fracture mode between

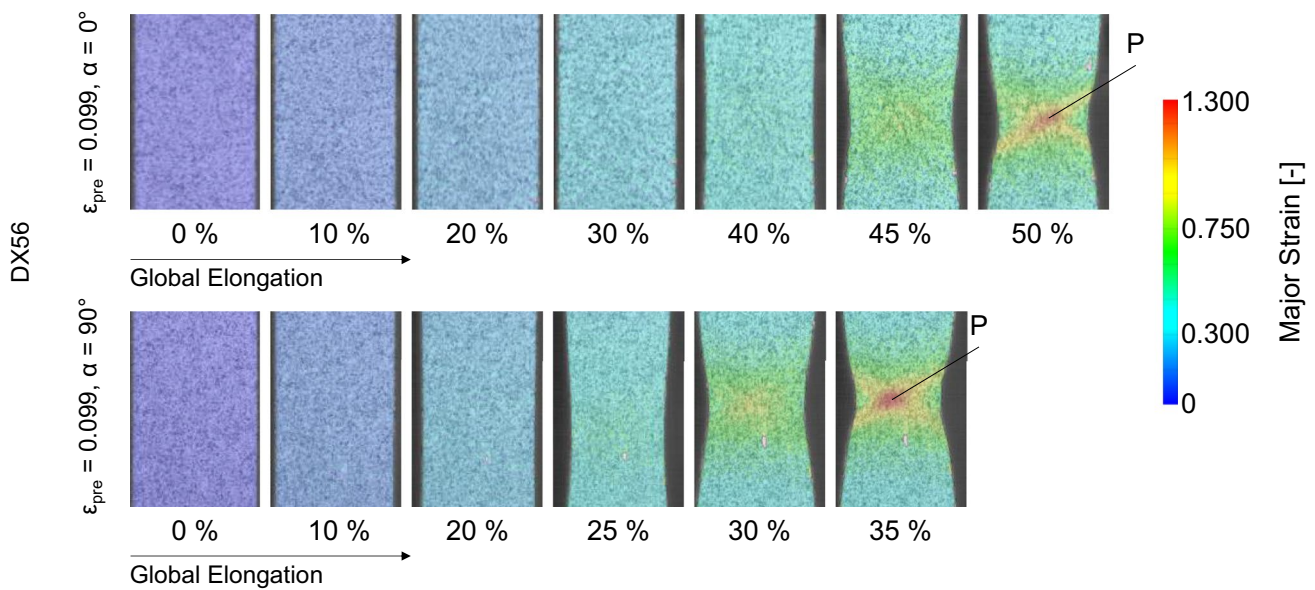
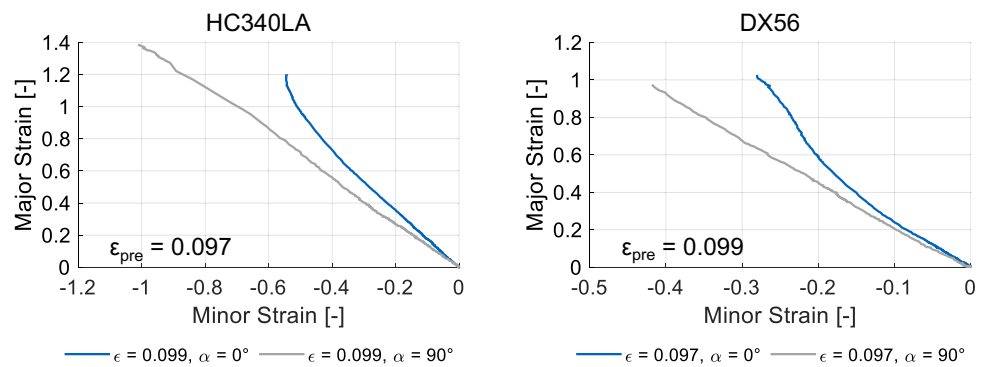


Fig. 9 Major Strain distribution for the DX56 tensile test with a pre-forming of $\epsilon = 0.099$ and an angle of $\alpha = 0^\circ$ and $\alpha = 90^\circ$, respectively. Point P indicates the evaluation point for the strain path

Fig. 10 Strain path for point P of the specimens shown in Fig. 9



ductile and brittle fracture can be observed. Where the specimen with no change in loading direction ($\alpha = 0^\circ$) show only small voids. For the DX56 a ductile failure in combination with shear mechanisms can be observed for specimens with low pre-forming heights. Higher pre-forming leads to an increase of the shear mechanisms for $\alpha = 0^\circ$ and $\alpha = 90^\circ$ specimens and reduced ductile failure mechanisms. Nevertheless, a change in loading direction leads to higher amounts of shear mechanisms and increased void size compared to the specimen with no change in loading direction. Therefore, a lower triaxiality and a positive Lode parameter are present during failure. The combination of a low triaxiality and a positive Lode parameter lead to concentrated plastic strain zones around the voids. The void coalescence is dominated by shearing, see Zhu et al. [34]. This findings are in good agreement with the SEM findings for the fracture

surfaces of pre-formed Nakajima experiments by Volk et al. [30].

Nanoindentation results

To ascertain the effect of pre-forming on the microstructure, microstructural analysis and nanoindentation of single grains as well as the grain boundaries are conducted. For the inverse calculation of the flow curves the pre-straining heights of $\epsilon_{pre} = 0.046$ and $\epsilon_{pre} = 0.097$ for the HC340LA steel and $\epsilon_{pre} = 0.046$ and $\epsilon_{pre} = 0.099$ for the DX56 steel are chosen. The lower pre-forming height is just under the critical pre-forming height and the higher pre-forming height is the height where a significant loss of formability can be observed.

The experiments revealed, that the grain boundaries have a higher hardness than the grains which also leads to different indentation depth, respectively (Fig. 12). The

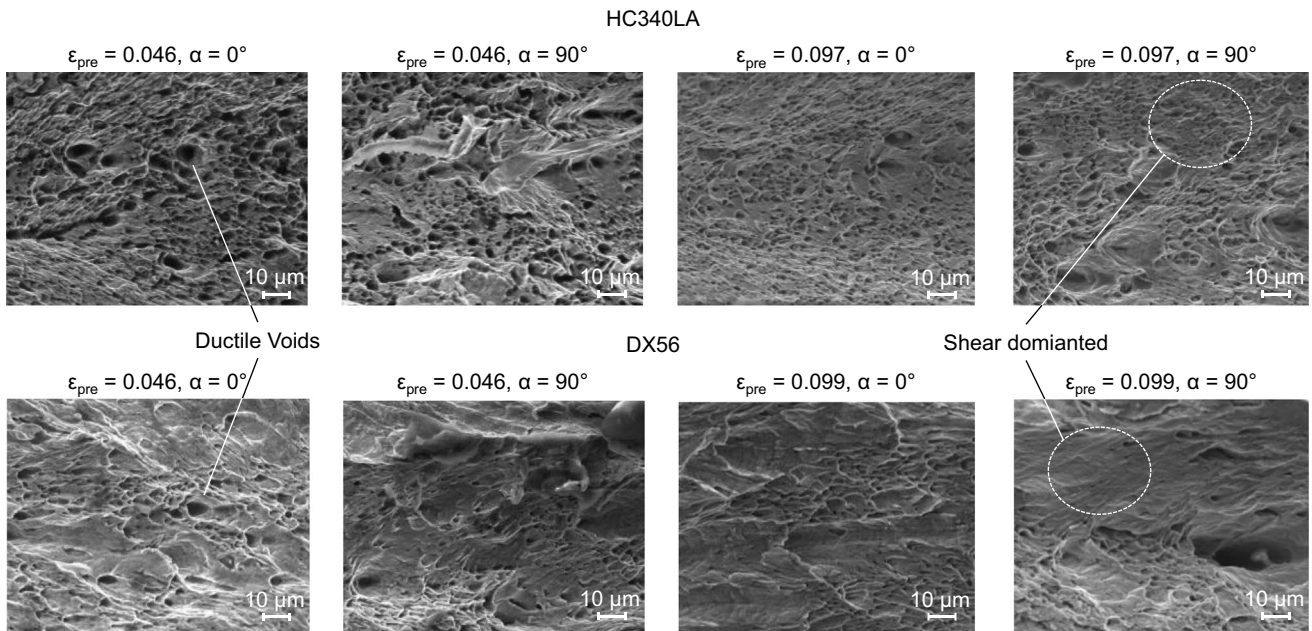


Fig. 11 SEM—images of the fracture surfaces for DX56 and HC340LA under different pre-forming heights and loading directions with increased void sizes after a change in loading direction at increased pre-forming heights

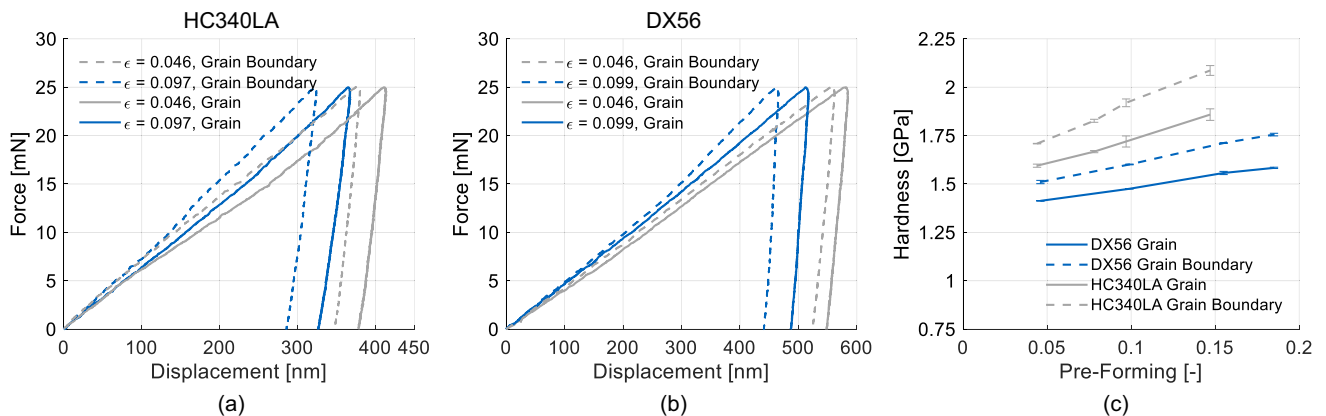


Fig. 12 Hysteresis curves of the investigated materials, (a) HC340LA, (b) DX56 and pre-forming heights and (c) the resulting average hardness over the pre-forming strain

hardness of different grains or grain boundaries show only a little deviation. By indenting the two different pre-forming heights, it is found, that grain boundaries also have a higher increase in strength than the ferrite grains when comparing the two pre-forming heights. For the numerical simulation, the force–displacement curves of experiments were chosen which have a hardness close to the average hardness, which is shown in Fig. 12 (c).

Ohmura et al. [21] found a similar behaviour for an interstitial-free steel. They also observed, that an indent close to the grain boundary or on the grain boundary also has an increased hardness in comparison to the centre

of the grain and that the nanohardness of two different grains is quite similar. For the experiments conducted in this study, the amount of pre-forming also changes the force–displacement curves. A higher pre-strain leads to a bigger difference in between the hardness of the grains and the grain boundary (Fig. 15). As a smaller grain size leads to an increase in strength, the force–displacement curves for the HC340LA steel are above those from the DX56 steel. This is in good agreement with the observations from nanoindentation experiments with two different steels with varying grain size of Miyahara et al. [20] (Fig. 13).

These results are used to inverse calibrate the flow curve for the pre-formed materials. By iterative adjustment of the flow curve the difference between the experimental and the numerical results were minimized and the flow curves for the grains and the grain boundaries were determined. The flow curve is modelled by the Swift approach, which is chosen due to its low number of parameters which have to be fitted. The three parameters

C , ϵ_0 and m are optimized until the average deviation between the experimental force–displacement curve and the numerical force–displacement curve is below 5%, see Fig. 14. The 5% boundary was already used by Dias and Godoy [7], leading to a sufficient accuracy in the determination of the parameters.

To minimize the time effort and to make use of the symmetric experimental setup, only a quarter of the

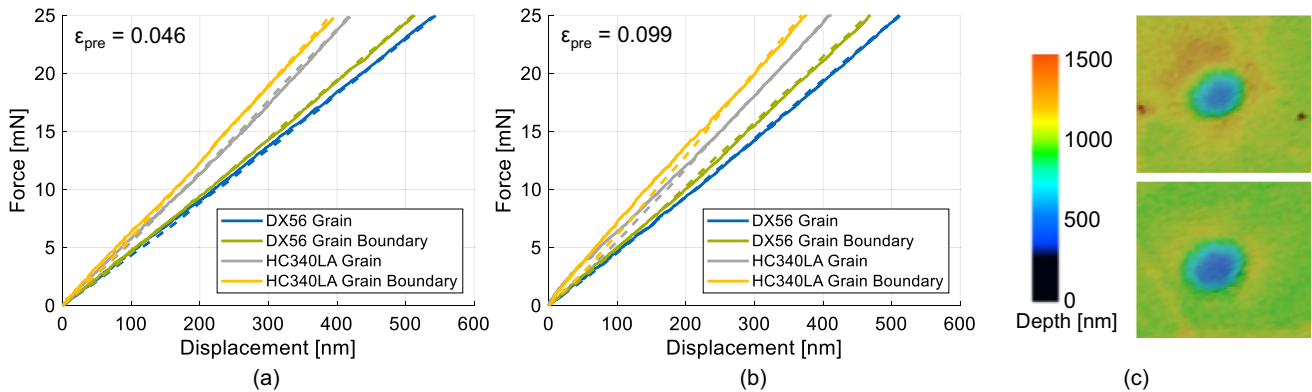


Fig. 13 Experimental and numerical Force–Displacement curves from nanoindentation at two pre-form heights (a) $\epsilon=0.046$ and (b) $\epsilon=0.099$ were the dashed lines represent the simulated results. (c)

Resulting indents depths on a grain boundary (upper picture) and inside a grain (lower picture)

Fig. 14 Fitting procedure for the Swift-parameters

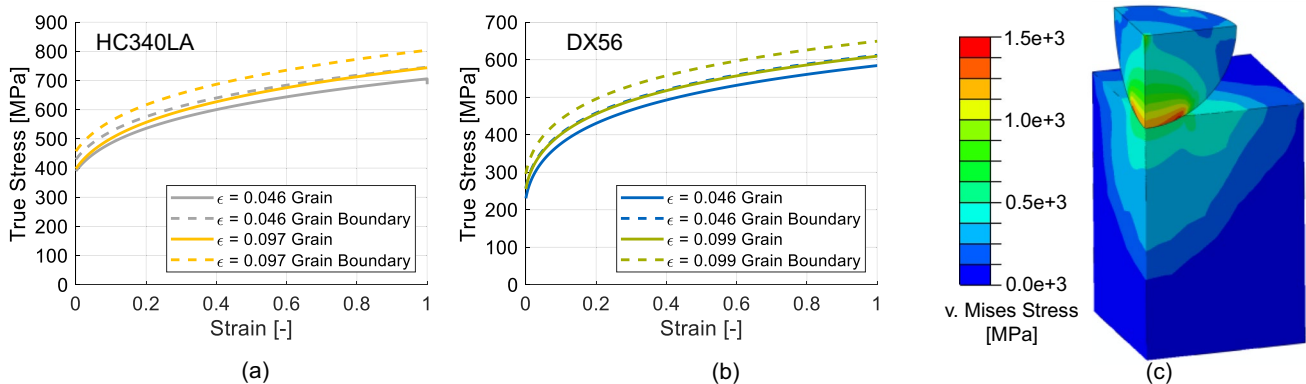
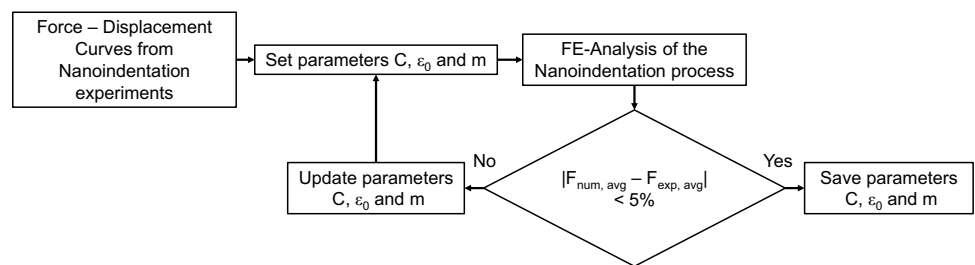


Fig. 15 Flow curves obtained by inverse parameter identification for (a) HC340LA and (b) DX56 and (c) the used simulation model

Table 2 Swift-parameters for the different materials and pre-forming heights

	Pre-Forming	Phase	C	ϵ_0	m
HC340LA	0.046	Grain	737.3	0.04574	0.2
	0.046	Grain Bound-ary	737.3	0.12574	0.19
	0.097	Grain	750.0	0.04574	0.15
	0.097	Grain Bound-ary	824.6	0.04888	0.1179
DX56	0.046	Grain	585.0	0.007322	0.1948
	0.046	Grain Bound-ary	612.1	0.008534	0.1849
	0.099	Grain	609.7	0.008426	0.1858
	0.099	Grain Bound-ary	649.3	0.01009	0.173

punch and the material are simulated. As the punch radius is only 5.8 μm , very small element sizes have to be used. In the contact zone of the punch and the material, the element size of the 3D tetrahedron elements (C3D10M element type in ABAQUS) is set to 50 nm. Referable to the very small measured displacement, the elastic deformation of the spherical diamond punch has to be taken into account as well. Due to the small contact area of the punch and the material, stresses up to 1850 MPa can be observed at the tip of the punch, see Fig. 15. Therefore, the elastic deformation is simulated by applying a Young's modulus of 1141 GPa and it is assumed that no plastic deformation of the punch occurs based on the high yield strength of diamond of 130 GPa found by Eremets et al. [9]. The maximum elastic deformation of the punch is about 6.8 nm for the HC340LA grain boundary at a pre-forming of $\epsilon = 0.097$. By ignoring the elastic deformation, an error of 1.8% in displacement of the punch is made. In contrast to the indentation simulations of Dias and Godoy [7] and Casals and Alcalá [4], which assumed frictionless contact between the punch and the material, a friction coefficient of $\mu = 0.01$ is assumed. The stresses, strains and displacement of the material can be found in Appendix B.

The obtained Swift parameters for the flow curves from the FE-analysis can be found in Table 2. The young's modulus is set to $E = 210$ GPa for all materials and pre-forming heights.

Conclusion

In this study, two single-phase ferrite steels, HC340LA and DX56, were subjected to tensile tests after pre-forming. Six different pre-forming heights, ranging from $\epsilon = 0.01$ up to $\epsilon = 0.15$ for the HC340LA steel and $\epsilon = 0.02$ up to $\epsilon = 0.18$ for the DX56 steel were investigated. To investigate the influence of a change in loading direction after pre-forming, the tests were conducted under 0° , 22.5° , 45° , 67.5° and 90° to the initial loading direction which was under 0° to the rolling direction. The experimental and numerical results lead to the following conclusions:

- The amount of pre-forming as well as a change in loading direction have a significant influence on the mechanical parameters as well as the formability for both investigated materials.
- SEM – images showed, that a change in the failure mode occurs for high pre-forming heights and a change in loading direction. The failure mode is changed from ductile fracture to a mixed mode between ductile and brittle fracture.
- By using nanoindentation and a following inverse parameter finding, the flow curves for the grains as well as the grain boundaries were determined. The grain boundaries show a higher strength than the grains and also a higher increase in strength during forming. For the fine-grained HC340LA steel, the hardness is higher than for the coarse-grained DX56 steel.

In the current study only single-phase steels have been investigated, so therefore further research is required to investigate the effects for materials with two or more phases or inclusions as well as other materials like aluminium alloys where the strength of the material is caused by other mechanisms than grain boundaries.

Appendix A. Additional experimental data

Table 3

Table 3 Rp0.2% in MPa dependent on the pre-forming height and the angle α for DX56

Angle α [°]	Pre-Forming [-]					
	0.022	0.046	0.065	0.095	0.155	0.185
0°	204.89	239.29	256.85	290.96	319.94	332.3
22.5°	214.09	247.78	274.15	304.71	334.62	349.9
45°	223.86	260.98	292.21	323.82	366.51	376.47
67.5°	214.21	247.59	273.48	299.43	345.39	359.16
90°	200.77	231.08	258.31	285.83	320.33	328.93

Table 4

Table 4 Rp0.2% in MPa dependent on the pre-forming height and the angle α for HC340LA

Angle α [°]	Pre-Forming [-]					
	0.011	0.044	0.078	0.097	0.123	0.147
0°	338.04	412.41	453.81	473.62	494.39	531.63
22.5°	342.04	406.19	453.22	472.49	491.66	494.19
45°	355.63	415.49	455.36	453.87	497.92	524.41
67.5°	357.91	415.94	455.19	485.36	500.93	535.15
90°	354.60	415.74	454.61	484.22	510.48	500.88

Table 5

Table 5 Uniform Elongation dependent on the pre-forming height and the angle α for DX56

Angle α [°]	Pre-Forming [-]					
	0.022	0.046	0.065	0.095	0.155	0.185
0°	0.222	0.198	0.176	0.138	0.073	0.047
22.5°	0.228	0.202	0.177	0.009	0.006	0.005
45°	0.219	0.194	0.159	0.006	0.005	0.005
67.5°	0.222	0.202	0.169	0.008	0.008	0.008
90°	0.232	0.220	0.179	0.012	0.010	0.010

Table 6

Table 6 Uniform Elongation dependent on the pre-forming height and the angle α for HC340LA

Angle α [°]	Pre-Forming [-]					
	0.022	0.046	0.065	0.095	0.155	0.185
0°	0.179	0.133	0.099	0.072	0.039	0.002
22.5°	0.177	0.138	0.058	0.006	0.006	0.006
45°	0.174	0.128	0.007	0.007	0.006	0.006
67.5°	0.169	0.127	0.009	0.008	0.007	0.008
90°	0.169	0.129	0.011	0.009	0.009	0.011

Table 7

Table 7 Fracture Elongation dependent on the pre-forming height and the angle α for DX56

Angle α [°]	Pre-Forming [-]					
	0.022	0.046	0.065	0.095	0.155	0.185
0°	0.413	0.394	0.372	0.353	0.267	0.274
22.5°	0.408	0.387	0.375	0.321	0.199	0.130
45°	0.395	0.369	0.349	0.245	0.124	0.092
67.5°	0.394	0.379	0.361	0.277	0.112	0.111
90°	0.413	0.408	0.389	0.283	0.139	0.116

Table 8

Table 8 Fracture Elongation dependent on the pre-forming height and the angle α for HC340LA

Angle α [°]	Pre-Forming [-]					
	0.022	0.046	0.065	0.095	0.155	0.185
0°	0.293	0.256	0.227	0.214	0.187	0.123
22.5°	0.291	0.255	0.225	0.123	0.107	0.109
45°	0.299	0.275	0.154	0.129	0.077	0.054
67.5°	0.281	0.259	0.121	0.079	0.067	0.049
90°	0.283	0.237	0.120	0.084	0.068	0.053

Appendix B. Additional simulation data

Figure 16

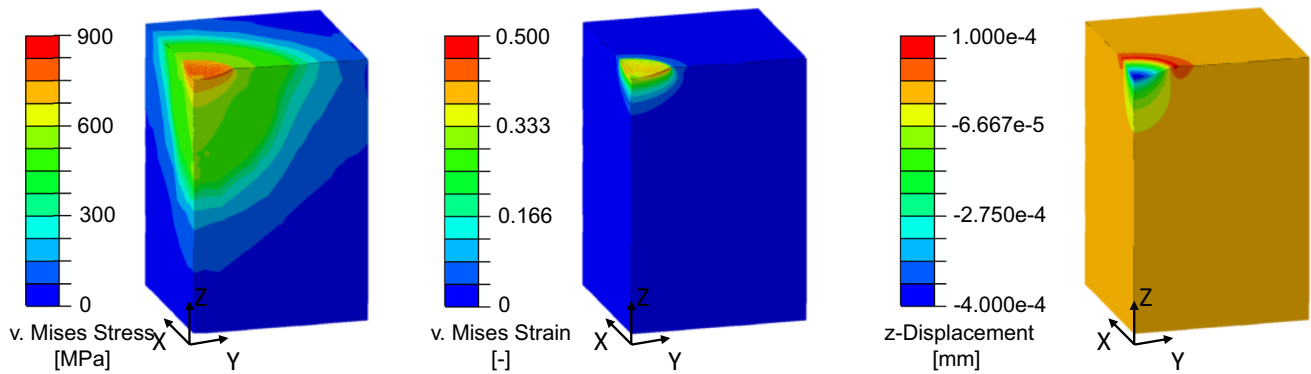


Fig. 16 v. Mises stress, v. Mises Strain and the displacement in z for a nanoindentation simulation

Acknowledgements The authors would like to thank the German Research Foundation (DFG) for their financial support under the grant numbers 429432653, 455960756 and 374548845.

Funding Open Access funding enabled and organized by Projekt DEAL.

Declarations

Conflict of interest The authors declare that they have no conflict of interest.

Open Access This article is licensed under a Creative Commons Attribution 4.0 International License, which permits use, sharing, adaptation, distribution and reproduction in any medium or format, as long as you give appropriate credit to the original author(s) and the source, provide a link to the Creative Commons licence, and indicate if changes were made. The images or other third party material in this article are included in the article's Creative Commons licence, unless indicated otherwise in a credit line to the material. If material is not included in the article's Creative Commons licence and your intended use is not permitted by statutory regulation or exceeds the permitted use, you will need to obtain permission directly from the copyright holder. To view a copy of this licence, visit <http://creativecommons.org/licenses/by/4.0/>.

References

1. Barlat F, Ferreira Duarte JM, Gracio JJ, Lopes AB, Rauch EF (2003) Plastic flow for non-monotonic loading conditions of an aluminum alloy sheet sample. *Int J Plast* 19(8):1215–1244. [https://doi.org/10.1016/S0749-6419\(02\)00020-7](https://doi.org/10.1016/S0749-6419(02)00020-7)
2. Barlat F, Gracio JJ, Lee M-G, Rauch EF, Vincze G (2011) An alternative to kinematic hardening in classical plasticity. *Int J Plast* 27(9):1309–1327. <https://doi.org/10.1016/j.ijplas.2011.03.003>
3. Bergström Y, Ölund S (1982) The forming limit diagram of sheet metals and effects of strain path changes on formability: a dislocation treatment. *Mater Sci Eng* 56(1):47–61. [https://doi.org/10.1016/0025-5416\(82\)90181-1](https://doi.org/10.1016/0025-5416(82)90181-1)
4. Casals O, Alcalá J (2005) The duality in mechanical property extractions from Vickers and Berkovich instrumented indentation experiments. *Acta Mater* 53(13):3545–3561. <https://doi.org/10.1016/j.actamat.2005.03.051>
5. Choi B-W, Seo D-H, Yoo J-Y, Jang J-I (2009) Predicting macroscopic plastic flow of high-performance, dual-phase steel through spherical nanoindentation on each microphase. *J Mater Res* 24(3):816–822. <https://doi.org/10.1557/jmr.2009.0109>
6. Clausmeyer T, Gerstein G, Bargmann S, Svendsen B, van den Boogaard AH, Zillmann B (2013) Experimental characterization of microstructure development during loading path changes in bcc sheet steels. *J Mater Sci* 48(2):674–689. <https://doi.org/10.1007/s10853-012-6780-9>
7. Dias AMS, Godoy GCD (2010) Determination of stress-strain curve through berkovich indentation testing. *MSF* 636–637:1186–1193. <https://doi.org/10.4028/www.scientific.net/MSF.636-637.1186>
8. DIN Deutsches Institut für Normung e. V (2016) Testing of metallic materials – Tensile test pieces. Beuth, Berlin
9. Eremets MI, Trojan IA, Gwaze P, Huth J, Boehler R, Blank VD (2005) The strength of diamond. *Appl Phys Lett* 87(14):141902. <https://doi.org/10.1063/1.2061853>
10. Graf A, Hosford W (1993) Effect of Changing Strain Paths on Forming Limit Diagrams of Al2008-T4. *MTA* 24(11):671. <https://doi.org/10.1007/BF02646529>
11. Hora P, Tong L (2006) Numerical prediction of FLC using the enhanced modified maximum force criterion (eMMFC). *Proc FLC* 2006:31–36
12. Hora P, Tong L, Berisha B (2013) Modified maximum force criterion, a model for the theoretical prediction of forming limit curves. *Int J Mater Form* 6(2):267–279. <https://doi.org/10.1007/s12289-011-1084-1>
13. Hora P, Tong L, Reissner J (1996) A prediction method for ductile sheet metal failure in FE-simulation. *Numisheet* 1996:252–256
14. Kim H, Barlat F, Lee Y, Zaman SB, Lee CS, Jeong Y (2018) A crystal plasticity model for describing the anisotropic hardening behavior of steel sheets during strain-path changes. *Int J Plast* 111(14):85–106. <https://doi.org/10.1016/j.ijplas.2018.07.010>
15. Kim J-Y, Kang S-K, Greer JR, Kwon D (2008) Evaluating plastic flow properties by characterizing indentation size effect using a sharp indenter. *Acta Mater* 56(14):3338–3343. <https://doi.org/10.1016/j.actamat.2008.02.049>
16. Larsson R, Björklund O, Nilsson L, Simonsson K (2011) A study of high strength steels undergoing non-linear strain paths—Experiments and modelling. *J Mater Process Technol* 211(1):122–132. <https://doi.org/10.1016/j.jmatprotec.2010.09.004>
17. Lebensohn RA, Tomé CN (1993) A self-consistent anisotropic approach for the simulation of plastic deformation and texture development of polycrystals: Application to zirconium alloys. *Acta Metall Mater* 41(9):2611–2624. [https://doi.org/10.1016/0956-7151\(93\)90130-K](https://doi.org/10.1016/0956-7151(93)90130-K)
18. Manopulo N, Hora P, Peters P, Gorji M, Barlat F (2015) An extended Modified Maximum Force Criterion for the prediction of localized necking under non-proportional loading. *Int J Plast* 75(5–8):189–203. <https://doi.org/10.1016/j.ijplas.2015.02.003>
19. Merklein M, Suttner S, Brosius A (2014) Characterisation of kinematic hardening and yield surface evolution from uniaxial to biaxial tension with continuous strain path change. *CIRP Ann* 63(1):297–300. <https://doi.org/10.1016/j.cirp.2014.03.039>
20. Miyahara K, Matsuoka S, Hayashi T (2001) Nanoindentation as a strength probe—a study on the hardness dependence of indent size for fine-grained and coarse-grained ferritic steel. *Metall and Mat Trans A* 32(13):761–768. <https://doi.org/10.1007/s11661-001-1010-0>
21. Ohmura T, Tsuzaki K, Yin F (2005) Nanoindentation-Induced Deformation Behavior in the Vicinity of Single Grain Boundary of Interstitial-Free Steel. *Mater Trans* 46(9):2026–2029. <https://doi.org/10.2320/matertrans.46.2026>
22. Seok M-Y, Kim Y-J, Choi I-C, Zhao Y, Jang J-I (2014) Predicting flow curves of two-phase steels from spherical nanoindentation data of constituent phases: Isostrain method vs. non-isostrain method. *Int J Plast* 59:108–118. <https://doi.org/10.1016/j.ijplas.2014.03.013>
23. Stoughton TB (2000) A general forming limit criterion for sheet metal forming. *Int J Mech Sci* 42(1):1–27. [https://doi.org/10.1016/S0020-7403\(98\)00113-1](https://doi.org/10.1016/S0020-7403(98)00113-1)
24. Stoughton TB, Yoon JW (2012) Path independent forming limits in strain and stress spaces. *Int J Solids Struct* 49(25):3616–3625. <https://doi.org/10.1016/j.ijsolstr.2012.08.004>
25. Tarigopula V, Hopperstad OS, Langseth M, Clausen AH (2008) Elastic-plastic behaviour of dual-phase, high-strength steel under strain-path changes. *Eur J Mech A Solids* 27(5):764–782. <https://doi.org/10.1016/j.euromechsol.2008.01.002>
26. Vincze G, Butuc MC, Barlat F, Lopes AB, Silva TFV (2019) Strain path changes in aluminum. In Proceedings of the 22nd International Esaform Conference on Material Forming: Esaform 2019, Vitoria-Gasteiz, Spain. 8–10 May 2019. AIP Publishing, p. 160013

27. Volk W, Gruber M, Norz R (2020a) Prediction of limit strains during non-proportional load paths with a change in loading direction. IOP Conf Ser: Mater Sci Eng 967. <https://doi.org/10.1088/1757-899X/967/1/012069>
28. Volk W, Hoffmann H, Suh J, Kim J (2012) Failure prediction for nonlinear strain paths in sheet metal forming. CIRP Ann 61(1):259–262. <https://doi.org/10.1016/j.cirp.2012.03.111>
29. Volk W, Hora P (2011) New algorithm for a robust user-independent evaluation of beginning instability for the experimental FLC determination. Int J Mater Form 4(3):339–346. <https://doi.org/10.1007/s12289-010-1012-9>
30. Volk W, Norz R, Eder M, Hoffmann H (2020b) Influence of non-proportional load paths and change in loading direction on the failure mode of sheet metals. CIRP Ann 69(1):273–276. <https://doi.org/10.1016/j.cirp.2020.03.009>
31. Volk W, Suh J (2013) Prediction of formability for non-linear deformation history using generalized forming limit concept (GFLC). In NUMISHEET 2014: The 9th International Conference and Workshop on Numerical Simulation of 3D Sheet Metal Forming Processes: Part A Benchmark Problems and Results and Part B General Papers, Melbourne, Australia. 6–10 January 2014. AIP, pp. 556–561.
32. Weinschenk A, Volk W (2017) FEA-based development of a new tool for systematic experimental validation of nonlinear strain paths and design of test specimens. AIP Conf Proc 1896. <https://doi.org/10.1063/1.5007966>
33. Zaman SB, Barlat F, Kim J-H (2018) Deformation-induced anisotropy of uniaxially prestrained steel sheets. Int J Solids Struct 134(11):20–29. <https://doi.org/10.1016/j.ijsolstr.2017.10.029>
34. Zhu Y, Engelhardt MD, Kiran R (2018) Combined effects of triaxiality, Lode parameter and shear stress on void growth and coalescence. Eng Fract Mech 199(5):410–437. <https://doi.org/10.1016/j.engfracmech.2018.06.008>

Publisher's note Springer Nature remains neutral with regard to jurisdictional claims in published maps and institutional affiliations.